Anisotropic Heisenberg model close to the Ising limit: Triangular lattice versus effective models

M. Ulaga [1,*] J. Kokalj [2,3] T. Tohyama [4] and P. Prelovšek [3]

[1] *Max Planck Institute for the Physics of Complex Systems, 01087 Dresden, Germany*

[2] *Faculty of Civil and Geodetic Engineering, University of Ljubljana, SI-1000 Ljubljana, Slovenia*

[3] *Jožef Stefan Institute, SI-1000 Ljubljana, Slovenia*

[4] *Department of Applied Physics, Tokyo University of Science, Tokyo 125-8585, Japan*

(Received 14 October 2025; revised 3 January 2026; accepted 12 June 2026; published 8 July 2026)

Stimulated by recent experiments on materials representing the realization of the anisotropic Heisenberg spin-1/2 model on a triangular lattice (TL), we explore further properties of such a model in the easy-axis regime $\alpha = J_\perp/J_z < 1$ and the plausibility of finding effective models that capture similar physics. We show that, at finite fields, the magnetization curve as well as the transverse magnetization (superfluid) order parameter $m_\perp$ of the TL model are indeed qualitatively reproduced by anisotropic Heisenberg models on the honeycomb or square lattice. At the point of correspondence to the zero-field TL model, however, the bipartite models are qualitatively different, as they remain gapless even at $\alpha \ll 1$ with a small but finite $m_\perp > 0$. Conversely, we present several additional numerical studies of the full model on the TL which support the appearance of a gap at zero field and $\alpha \ll 1$. The magnetization curve $m(h)$ and the spin stiffness ρ_s indicate a transition/crossover from gapless to gapped regimes at $\alpha \sim \alpha^*$, with $\alpha^* \lesssim 0.5$. We also show that deviations from the linear spin-wave theory and the emergence of the gap can be traced back to the strong effective repulsion between magnon excitations, showcasing similarity to strongly correlated systems.

DOI: 10.1103/f5xy-9q3m

I. INTRODUCTION

The antiferromagnetic (AFM) Heisenberg spin-1/2 model on the triangular lattice (TL) has been a source of many theoretical concepts as well as challenges. The isotropic case was proposed as the model for the phenomenon of quantum spin liquid [1] but later shown to exhibit a nontrivial broken translational symmetry in the ground state (gs) with tripling of the unit cell and 120° alignment of spins [2,3], which was already a challenge for powerful numerical approaches [4,5]. The anisotropy $\alpha = J_\perp/J_z$ in the easy-axis regime $|\alpha| < 1$ opens another set of phenomena. While the Ising limit with $\alpha = 0$ has been solved analytically to reveal a finite entropy at $T = 0$ [6], the regime $0 < |\alpha| < 1$, considered an interesting problem long ago [7], has emerged as the potential realization of the scenario of a (spin) supersolid [8], having (at least at $T = 0$) in addition to the broken translational symmetry and related diagonal magnetization $m_z > 0$ broken rotational symmetry with finite off-diagonal transverse magnetization $m_\perp > 0$. This possibility has been studied and established in the regime $\alpha < 0$ by several numerical studies [9–12], with apparently similar results for the AFM regime $\alpha > 0$ [12–15].

The strong additional momentum to theoretical considerations has recently been given by the synthesis and experiments on materials where the properties appear to be well represented by the AFM anisotropic Heisenberg model (AHM) on a TL with $0 < \alpha < 1$. While $Na_2BaCo(PO_4)_2$ [16–19], with $\alpha \sim 0.6$, seems to represent the spin system with properties close to the isotropic case and $NdTa_7O_{19}$ [20] is characterized by $\alpha \ll 1$ but small $J_z \sim 0.9$ K, the most promising material is $K_2Co(SeO_3)_2$ (KCSO) [21], with $\alpha \sim 0.07$ and $J_z \sim 35$ K, which has already allowed experimental studies of thermodynamic properties as well as dynamical spin excitations (via inelastic neutron scattering) in a wide range of temperatures and magnetic fields [22–24]. These experimental findings have already stimulated a series of additional (mostly numerical) theoretical studies [25–29].

While in many aspects these theoretical (model) calculations agree with experimental findings, the potential qualitative disagreement is the strict existence of the supersolid, i.e., of gapless excitations (and corresponding $m_\perp > 0$) in the AHM at $h = 0$ (without external magnetic field) close to the Ising limit, i.e., at $\alpha \ll 1$. The available numerical results for the supersolid parameter $m_\perp$ at $\alpha \ll 1$ indicate at least its very small value, being strongly dependent on applied finite-size scaling $N \to \infty$ [13,25–28]. This might indicate even a vanishing $m_\perp(h = 0) = 0$ [26,28], compatible with the interpretation with gapped magnon excitations $\Delta_1 > 0$ and discontinuous $T = 0$ magnetization curve $m(h < h^*) = 0$ [26], with $h^* \ll h_c$, where h_c denotes the onset of the $m = 1/3$ magnetization plateau well pronounced and extended in the $\alpha \ll 1$ regime. On the other hand, numerical studies as well as the experiment are consistent in the observation that $h^* < h < h_c$ induces supersolid $m_\perp > 0$.

Since the AHM on a TL in the $\alpha \ll 1$ regime at $T = 0$ reveals the tripling of the unit cell and large longitudinal

*Contact author: martinu@pks.mpg.de

Published by the American Physical Society under the terms of the Creative Commons Attribution 4.0 International license. Further distribution of this work must maintain attribution to the author(s) and the published article's title, journal citation, and DOI. Open access publication funded by Max Planck Society.

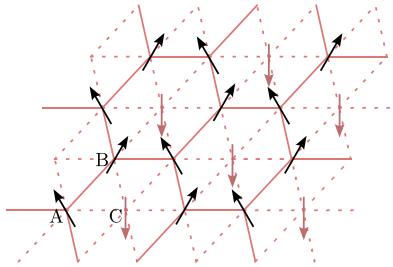


FIG. 1. An effective Heisenberg spin model on the HcL, where the translational symmetry on the TL is broken by fixing a third of spins of the classical Y state on the TL (sublattice C). The remaining two sublattices (AB) form a magnetized HcL under the effective field of the frozen spins.

magnetization $m_z > 0$, one might speculate that some properties of the full model can be reproduced within a reduced model, whereby breaking the translational symmetry, a third of spins are fixed in their maximum value, leading to an effective AHM on the honeycomb lattice (HcL) but in a finite field $h > 0$ [26], see Fig. 1 for an illustration. Since the latter lattice is (in contrast with the TL) bipartite, even the AHM on a square lattice (SqL) could be expected to have similar properties. We present here a detailed $T = 0$ numerical study of the corresponding magnetization curve $m(h)$ as well as $m_\perp$, which reveals a correspondence to the full TL regarding the anomalous behavior at $\alpha \ll 1$ and $h > 0$.

Still, despite this similarity, one clear message from studying the HcL and SqL is that, at the most interesting point of correspondence (to the TL with $h = 0$), a qualitative difference remains: Magnon excitations remain gapless on these bipartite models, and they possess a finite $m_\perp > 0$, although strongly reduced. Returning to the most challenging problem, i.e., the AHM on the TL and $h \sim 0$, we present additional evidence that, in the regime of $\alpha \ll 1$, we are dealing instead with a gapped solid, with the support emerging from numerical results for magnetization curves $m(h \sim 0)$ and for the spin stiffness ρ_s. Such a scenario naturally opens the question of the presumable disappearance of the gap and the onset of $m_\perp > 0$ with increasing α, particularly on approaching the isotropic gapless case $\alpha = 1$. Consistent with our previous limited evidence [25], our additional results indicate a qualitative change, i.e., a crossover/transition at $\alpha^* \lesssim 0.5$, which evidently remains a challenge for a proper phenomenological explanation and further numerical tests. On the other hand, the existence of gapped excitations at $0 < \alpha \ll 1$ also reopens the question on the relation to the regime $\alpha < 0$ where the supersolid scenario appears more firmly established [9–12,30]. We therefore extend our analysis to this regime, which despite apparent symmetry, also reveals qualitative differences.

Since theoretical and experimental results are frequently compared to the linear spin-wave theory (LSWT) [31], we also critically evaluate its feasibility to the AHM in the $\alpha \ll 1$ regime. It has already been recognized that, for the TL, the latter yields $m_\perp(h)$ monotonously increasing with decreasing $h < h_c$ [26] with evident discrepancy with numerically established vanishing [26,28] (or at least very small [27]) $m_\perp(h = 0)$, whereby the origin could be attributed to the strong repulsion/correlations between magnons [32,33], which still represents a challenge for adequate analytical analysis.

II. REFERENCE MODELS ON HcL AND SqL

We consider the AFM $S = 1/2$ AHM with the nearest-neighbor (nn) exchange $J_z = J$ and the easy-axis anisotropy $0 < \alpha \leqslant 1$, in the presence of a longitudinal magnetic field h,

$$H = J \sum_{\langle ij \rangle} \left[S_i^z S_j^z + \frac{\alpha}{2} (S_i^+ S_j^- + S_i^- S_j^+) \right] - h \sum_i S_i^z, \qquad (1)$$

on different lattices with nn interaction and N sites. While the main challenge remains the model on the TL, we first focus on the reduced model on the HcL. This emerges naturally as the representation of the full TL model by considering that, at $\alpha \ll 1$, there is broken translational symmetry (at least at $T = 0$) with tripling of the unit cell and a well-pronounced diagonal long-range order parameter $m_z = (1/N) \sum_i \exp(i \mathbf{q}_K \cdot \mathbf{R}_i) \langle S_i^z \rangle \neq 0$, where $\mathbf{q}_K = (4\pi/3, 0)$. Such a situation can be simulated by freezing/fixing one sublattice of spins on the TL to their maximum polarization $S_i = -S$ [26], as illustrated in Fig. 1 (see also Ref. [33]), which leads to the model in Eq. (1) on the HcL but at an additional effective field $\tilde{h} = zJS$, where $z = 3$ is a number of nn on the HcL. It should be noted that the correspondence of the HcL to the TL model becomes exact (at $\alpha \to 0$) at the magnetization plateau $m = S^z_{\rm tot}/(NS) = 1/3$ since, there, the $\uparrow\uparrow\downarrow$ spin pattern is the gs of the model on the TL and matches the ferromagnetic solution $S^z_{\rm tot} = SN$ and corresponding $m = S^z_{\rm tot}/(NS) = 1$ on the HcL. Starting from the $m = 1/3$ plateau, the qualitative correspondence persists for finite $\alpha > 0$, while the central question is to what extent the effective HcL model reflects the physics of the TL when the HcL magnetization is decreased to $m = 1/2$ [26], simulating $m = h = 0$ in the TL model. The HcL is a bipartite lattice with two sites per unit cell. This naturally opens the possible similarity of the AHM on an even simpler bipartite lattice, i.e., the AHM on the SqL [34], where $z = 4$, and the focus is on the properties at effective $h > 0$ or equivalently on magnetizations $1/2 \lesssim m < 1$.

A. Magnetization curves

Within the effective models on the HcL and SqL, we first consider and evaluate magnetization curves $m(h)$. As in the previous study of the AHM on the TL [26], the density matrix renormalization group (DMRG) calculation on finite-size lattices with N sites and with periodic boundary conditions (PBCs) is employed here to find gs energies E_k^0 in different magnetization sectors $k = S^z_{\rm tot}$. Results in Figs. 2(a) and 2(b) are obtained on the HcL with a rhombic cluster of $N_c = 6 \times 6$ unit cells (i.e., with $N = 2N_c = 72$ sites) and on the SqL with a square $N = 8 \times 8 = 64$ cluster (see Appendix A). From E_k^0 and magnetizations $m_k = k/(NS)$, the corresponding fields are then extracted as $h_k = (E^0_{k+1} - E^0_{k-1})/2$.

Results in Figs. 2(a) and 2(b) show $m(\tilde{h})$ vs renormalized fields $\tilde{h} = h/(zSJ)$ on the HcL (with the nn number $z = 3$) and the SqL ($z = 4$), respectively, for different $\alpha = 0.1, 0.2,$ and 0.5. The first observation is that, indeed, the results are qualitatively and even quantitatively similar with

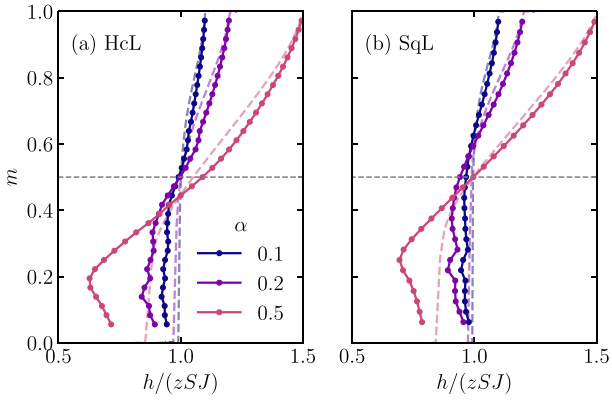


FIG. 2. Magnetization curves $m(h)$ vs renormalized fields $\tilde{h} = h/(zSJ)$ for (a) the HcL and (b) the SqL, for different anisotropies $\alpha = 0.1, 0.2,$ and 0.5, obtained with DMRG calculation on lattices with $N = 72$ and 64 sites, respectively. The black dashed lines indicate $m = 1/2$ and $\tilde{h} = 1$, corresponding to $m = 0$ and $h = 0$, respectively, within the TL model. The colored dashed lines represent the augmented LSWT results for $m(\tilde{h})$, discussed in Sec. IV.

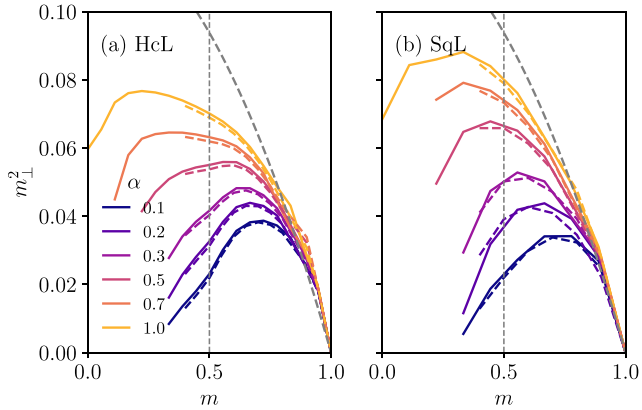


FIG. 3. Transverse order parameter $m_\perp^2$ vs magnetization m, extracted from ED results for DSSP on systems with $N = 36$ and 40 sites on (a) the HcL and (b) the SqL, for different $\alpha = 0.1$–1.0. Vertical $m = 1/2$ line indicates the correspondence to the $h = m = 0$ model on the TL. The gray dashed curve represents the expected LSWT dependence $m_\perp^2 = \zeta(1 - m^2)$, with $\zeta = 1/8$.

respect to the variation with α, considering different z. We note that, in the Ising limit $\alpha = 0$, the AFM solution becomes unstable to the ferrromagnetic one at $\tilde{h} = 1$ [35]. For the isotropic case with $\alpha = 1$ (not shown here), it has been established that, for the SqL, $m(h)$ is monotonously increasing from $h = 0$ to $h = h_c = 2J$ [36], and quite similar behavior is expected for the HcL. For $\alpha < 1$, there is a qualitative change at $h \to 0$ since magnon excitations in the AFM gs of the AHM at $h = 0$ become gapped with the magnon gap $\Delta_1 \sim zJS\sqrt{1-\alpha^2}$ [34]. This leads to the stable $m = 0$ solution for $h < h_1$ and for nonmonotonous (double solution) $m(h)$ in the regime $h_1 < h < h_2$. This instability regime (indicating a first-order transition of the gs with h) shrinks with decreasing $\alpha \to 0$, ending in a single step in $m(\tilde{h})$ in the Ising limit at $\tilde{h}_1 = \tilde{h}_2 = 1$.

Still, our focus is on the behavior at finite $\alpha > 0$ and the magnetization $m \gtrsim 1/2$, where the correspondence with the TL at $h \gtrsim 0$ is meaningful. In contrast with discontinuous $m(h < h^*) = 0$ (consistent with a magnon gap $\Delta_1 > 0$) found in the TL [26], in Fig. 2, it appears that, at $m \sim 1/2$, we have continuous $m(h)$ and $dm/dh > 0$ for both the HcL and SqL, i.e., there is no indication of a finite magnon gap. Conversely, the regime $m < 1/2$ is quite different on the HcL as well as on the SqL, revealing the (first-order) transition to the stable AFM $m = 0$ solution, also visible in Fig. 2 for all presented $\alpha < 1$.

We should comment here on the previous observation of anomalous excitations on the HcL at small $\alpha = 0.1$ and $m = 1/2$ [26]. They were obtained via exact diagonalization (ED) on smaller $N = 40$ as excited states within the same $S^z_{\rm tot}$, thus effectively representing two-magnon excitations, with $\omega_{\mathbf{q}}$ revealing an unusual upturn at the smallest q. The latter result is another manifestation of the delicate behavior of effective models at $m \sim 1/2$, which is shown here to persist for considerably larger N. The calculated $dm/dh > 0$ values are thus a more direct test against a possible finite magnon gap.

B. Transverse magnetization

In both effective models, one can expect at $T = 0$ and $h > 0$ broken rotational spin symmetry and corresponding order parameter, i.e., the transverse magnetization $m_\perp > 0$. We extract $m_\perp$ via the $T = 0$ transverse dynamical spin-structure factor (DSSF)

$$S^\perp(\mathbf{q}, \omega) = \langle\psi_0|S^x_{-\mathbf{q}}\delta(\omega - H + E_0)S^x_{\mathbf{q}}|\psi_0\rangle, \qquad (2)$$

evaluated within the gs wave function $|\psi_0\rangle$ for given spin sector $S^z_{\rm tot}$. Here, we calculate DSSF on the finite HcL and SqL with PBCs via ED, employing the Lanczos technique (see, e.g., Ref. [37]). Analyzing the lowest (soft) mode $\omega_{\mathbf{q}_0} = \Delta_1$ enables calculating the corresponding $S^\perp(\mathbf{q}_0, \omega) \sim A^\perp\delta(\omega - \Delta_1)$ and finally extracting $m_\perp^2 = A^\perp/N$. On the HcL, the relevant rotational-symmetry breaking appears at $\mathbf{q}_0 = (0, 0)$ with the (odd in each unit cell) spin operator $S^x_0 = N^{-1/2}\sum_i(S^x_{i1} - S^x_{i2})$, summed over all unit cells. Conversely, for the SqL, the soft mode is the zone-boundary one with $\mathbf{q}_0 = \mathbf{q}_M = (\pi, \pi)$ and the corresponding $S^x_{\mathbf{q}_M} = N^{-1/2}\sum_i e^{i\mathbf{q}_M\cdot\mathbf{R}_i}S^x_i$.

In Figs. 3(a) and 3(b), we present results for $m_\perp^2$ vs magnetization $m = 2S^z_{\rm tot}/N$, obtained via ED on $N = 36, 40$ sites for the HcL and SqL, shown within the whole range of anisotropies, $\alpha = 0.1$–1.0. The advantage of a smaller $N = 36$ is that, via ED, we can cover the whole range $0 \leqslant m \leqslant 1$, whereas for $N = 40$, we are limited (due to Hilbert-space dimension) to $m > 0.2$. Also, generally, we restrict in Figs. 3(a) and 3(b) our presentation to $m > m_*(\alpha)$ since the regime $m < m_*(\alpha)$ corresponds to the unstable regime in $m(h)$, and results become unphysical (as well as strongly size dependent).

Again, the qualitative behavior of $m_\perp^2(m)$ is quite similar for both the HcL and SqL. As expected, the dependence is quite generic, i.e., independent of α, for nearly saturated $m \lesssim 1$. There, one can give an explanation with the simplest classical result of the LSWT, where $m = \cos(\theta)$ and $m_\perp = S\sin(\theta)$ (note our different definitions of $m \leqslant 1$ and $m_\perp \leqslant 1/2$) and, consequently, $m_\perp^2 \propto 1 - m^2$. Still, deviations become very pronounced with decreasing $m < 1$ and $\alpha \ll 1$. At all α, the maximum of $m_\perp(m = m_0)$ is for $m = m_0 > 0$, a weak one

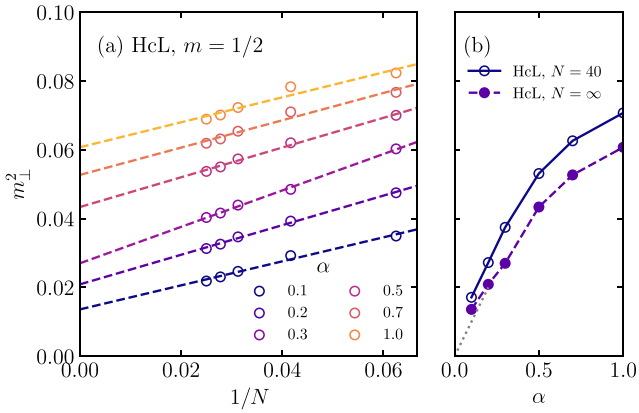


FIG. 4. Transverse order parameter $m_\perp^2$ at $m = 1/2$ for the HcL: (a) finite-size $1/N$ scaling of results for different α, (b) $m_\perp^2$, obtained on $N = 40$ sites, and extrapolated $N \to \infty$ values vs α.

even for the isotropic case $\alpha = 1$, with the value $m_\perp(h = m = 0) = 0.26$ for the SqL, being close to the established values [38]. On the other hand, the maximum becomes very pronounced for $\alpha < 0.5$, typically appearing at $m_0 > 0.5$.

Figure 4(a) presents the $1/N$ scaling of $m_\perp^2$ results for the HcL at the most interesting $m = 1/2$. In contrast with an analogous analysis for the TL, they reveal rather evident convergence to finite values even for the smallest $\alpha = 0.1$. In Fig. 4(b), we show $m_\perp^2$ vs α, both for $N = 40$ and extrapolated $N \to \infty$ values. The similarity to the TL is evident: For $\alpha \ll 1$, the pronounced maximum of $m_\perp(m)$ appears at intermediate $0.5 < m < 1$ (in contrast with LSWT prediction). However, a qualitative difference persists in the numerical results for $m_\perp(h = 0) \sim 0$ on the TL for $\alpha \ll 1$, extrapolating to much smaller values (essentially too small to be reliable) [26]. It is an open question why effective models still behave differently with respect to the gapped/gapless excitations at the point of correspondence. One evident and possibly crucial difference might emerge from the fact that the full model on TL at $h = 0$ has an inversion symmetry $m \to -m$, broken on the HcL and SqL at $m = 1/2$.

III. TL: EVOLUTION WITH ANISOTROPY

We turn back to the most challenging as well as experimentally most relevant case of the AHM on the TL at small $\alpha \ll 1$. Despite similarities with effective models at the point of correspondence (i.e., $m \sim 1/2$ for the HcL and SqL), there are qualitative differences with respect to the existence (or at least the size) of the transverse magnetization (supersolid parameter) $m_\perp > 0$ in the absence of an external field, at $h = 0$. As noticed already in several numerical studies of the $0 < \alpha \ll 1$ regime on the TL [13,26–28], the extracted values for $m_\perp$ are very sensitive to the finite-size extrapolation $N \to \infty$. In the following, we present some additional support for the scenario that, at $\alpha \ll 1$, we are dealing at $h = 0$ with the absence of supersolidity, i.e., $m_\perp = 0$ [26,28], which can be made compatible with the finite magnon gap $\Delta_1 > 0$. The most challenging question in this respect is the evolution of the behavior with increasing $\alpha \to 1$ since at least the gs of the isotropic case $\alpha = 1$ represents an ordered magnet with 120° spin alignment and gapless magnon excitations [3].

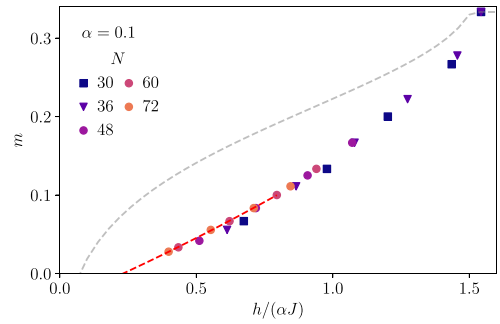


FIG. 5. Magnetization curve m vs normalized field $h/(\alpha J)$, for $\alpha = 0.1$, obtained with ED for $N = 30, 36$ lattices and via DMRG for $N = 48$–72 lattices, with the quadratic extrapolation (red dashed line). The black dashed line represents the result of LSWT, explained and discussed in Sec. IV.

A. Magnetization curves

A sensitive test of the possible gap is the magnetization curve $m(h)$ which is also a directly experimentally relevant quantity, at least for KCSO [24]. A finite magnon gap Δ_1 implies vanishing $m(h < h^* = \Delta_1) = 0$ at $T = 0$. For particularly $\alpha = 0.1$, the evidence for finite $h^* > 0$ has been presented with the previous calculations up to the $N = 60$ model on the TL [26]. Here, we extend the DMRG study to larger $N = 72$ but also to more systematic evolution with α including also $\alpha < 0$ for comparison. We present in Fig. 5 the results for $m(h)$ for the characteristic value $\alpha = 0.1$, obtained with ED for $N \leqslant 36$ and DMRG for $N = 48, 60$, and 72 (restricted to $S^z_{\rm tot} \leqslant 4$). A more systematic analysis of the evolution of $m(h \to 0)$ with anisotropy $\alpha \leqslant 1$, including also $\alpha = -0.1, -0.2$, is delegated to Appendix B. The presentation in terms of renormalized $h/(\alpha J)$ reveals a quite similar dependence, apart from the crucial regime $h \to 0$. Regarding the latter, there is clear evidence that the extrapolated results would be consistent with quite different marginal fields (effective magnon gaps) $h^* = \Delta_1 = \zeta \alpha J$, as summarized in Fig. 6. Results indicate that renormalized $h^*/(\alpha J) = \zeta$ is strongly reduced at intermediate $\alpha^* \sim 0.5$, which is an indication of a transition or crossover to a gapless regime. We should also point out a clear asymmetry with respect to the sign

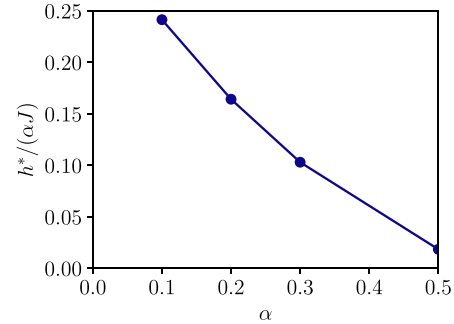


FIG. 6. Scaled gap $h^*/(\alpha J)$ vs α, as obtained by extrapolation of $m(h)$ results presented in Fig. 5 and in Appendix B.

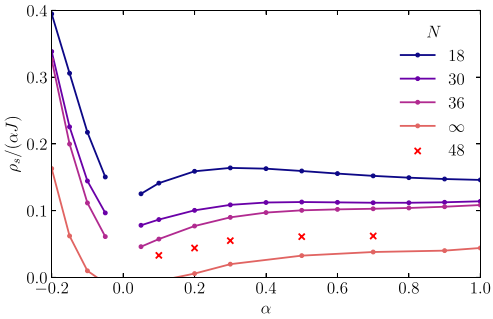


FIG. 7. Normalized spin stiffness $\rho_s/(\alpha J)$ vs anisotropy α, as calculated on the TL via ED on systems with different sizes $N = 18$, 30, and 36, together with the extrapolated value $N \to \infty$, obtained via the $1/N$ scaling. Crosses denote DMRG results on $N = 48$ sites.

of $\pm\alpha$ since at least $\alpha = -0.2$ (less clear for $\alpha = -0.1$) is, as expected [9–12], consistent with gapless excitations and consequently supersolid order.

B. Spin stiffness

Another important measure and test of the gs character is the spin stiffness ρ_s, representing the sensitivity of the supersolid order parameter $m_\perp$ to a twist in boundary conditions [13,30]. In finite-size calculations, it can be evaluated by introducing in Eq. (1) a phase $\theta_{ij} = \theta\ \mathbf{e}_\theta \cdot \mathbf{R}_{ij}$ into the spin exchange term

$$\tilde{H}_{\rm ex} = \frac{1}{2} J\alpha \sum_{\langle ij \rangle} [e^{i\theta_{ij}} S_i^+ S_j^- + e^{-i\theta_{ij}} S_i^- S_j^+]. \tag{3}$$

The spin stiffness is then calculated as $\rho_s = (1/N)\partial^2 E_0/\partial^2\theta$ [39–41]. In analogy to the charge stiffness [42] and the superfluid stiffness [43], finite $\rho_s > 0$ indicates gapless excitations, while $\rho_s = 0$ is the signature of a gapped system.

We present in Fig. 7 results for renormalized $\rho_s/(\alpha J)$ vs α, including also the range $\alpha < 0$, obtained within the ED approach by applying small $\theta \sim 0.1$ in the x direction as well those obtained via DMRG on $N = 48$ sites. The results in Fig. 7 reveal quite significant finite-size dependence (decrease) of calculated ρ_s with the system size N. Still, for the isotropic case $\alpha = 1$, the $1/N$ extrapolation yields finite-value $\rho_s \sim 0.05J$, well consistent with previous results for the TL [41]. For the present study, the most interesting and challenging aspect is the development of normalized $\rho_s/(\alpha J)$, particularly its extrapolated value, with α. As evident in Fig. 7, the variation is quite modest for $\alpha > 0.4$. However, there is a qualitative change at $\alpha < \alpha^* \sim 0.2$, indicating a vanishing $\rho_s = 0$, which can be compatible with the onset of finite gap $\Delta_1 > 0$. In this respect, results in the $\alpha < 0$ regime are also quite informative: Some similarity is visible (e.g., finite-size sensitivity) but also a pronounced asymmetry with the regime with $\alpha > 0$, visible even for small $\alpha = \pm 0.1$.

IV. LSWT: QUALITATIVE AGREEMENT VS FAILURE

To discuss the discrepancy between the numerically established gap on TL at $h = 0$ and gapless spin waves predicted by LSWT, we perform LSWT calculations by mainly following Ref. [31]. After obtaining classical ground states with three (A, B, and C) or two sublattices (A, B) on the TL or the SqL and HcL, respectively (see also Fig. 1), one performs bosonisation and writes the Hamiltonian in terms of bosonic operators $(a_i, a_i^\dagger)$.

Let us start the discussion at $h = h_c = 3\alpha SJ$, i.e., at the magnetization plateau on the TL, where the LSWT works best. In such a case, the classical angles of spins for the z axis for each sublattice are $\theta_A = \pi$, $\theta_B = \theta_C = 0$, which leads to a simplified analysis. Then the exchange term between site i on the A sublattice and site j on the B (or C) sublattice (for antiparallel spins) reads

$$H_{J,AB} = -\alpha JS(a_i a_j + a_i^\dagger a_j^\dagger) + JS(a_i^\dagger a_i + a_j^\dagger a_j) - J a_i^\dagger a_i a_j^\dagger a_j - JS^2. \tag{4}$$

Similarly, one obtains the exchange term between site i on the B sublattice and site j on the C sublattice (for parallel spins)

$$H_{J,BC} = \alpha JS(a_i a_j^\dagger + a_i a_j^\dagger) - JS(a_i^\dagger a_i + a_j^\dagger a_j) + J a_i^\dagger a_i a_j^\dagger a_j + JS^2. \tag{5}$$

The Hamiltonian $H_{J,BC}$ contains a hopping term on the HcL, yielding an almost exact description of the one-magnon excitation (lower-branch dispersion [25]) at the $m = 1/3$ plateau. This term is also governing the small number of magnon excitations, which are realized at reduced $m < 1/3$. However, when approaching $m \sim 0$, the number of magnons increases, and other terms become important. Among them, a strong repulsion term $J a_i^\dagger a_i a_j^\dagger a_j$ can play a significant role, making the system strongly interacting/correlated. It is, however, neglected within the standard LSWT.

We perform standard LSWT calculations on the HcL, SqL, and TL to evaluate the magnetization curves $m(h)$. For each h, we first calculate the classical gs and then include quantum corrections following Ref. [44] to obtain $E_0(h)$ and, from it, the magnetization m as $dE_0(h)/dh$. In contrast with the classical solution alone (which for $\alpha \ll 1$ evidently does not produce a proper m away from the plateau regime), the obtained magnetization is shown in Figs. 2 and 5 and agrees qualitatively well with the full numerical calculations of the model. It can be expected that the agreement is best close to the magnetization saturation or plateau, where only a small number of magnons are present in the system; therefore, higher-order terms, including magnon-magnon interactions, play only a minor role. The agreement close to $m = 1$ on the SqL and HcL in Fig. 2 is indeed very good. As one moves to $m < 1$, or $m < 1/3$ on the TL, respectively, the discrepancy becomes larger, particularly for $\alpha \ll 1$, since the neglected magnon-magnon interactions beyond LSWT become more relevant. On the TL, there is also a marked discrepancy at $h \sim 0$ since LSWT predicts negative m. This can be traced back to the overestimate of the quantum corrections to the classical result.

V. DISCUSSION

In this paper, we present further results relevant for the anisotropic easy-axis Heisenberg model on the TL. We first show that some relevant features of the full model are also reproduced on reduced models, obtained via explicitly breaking the translational symmetry by fixing a third of the spins. This

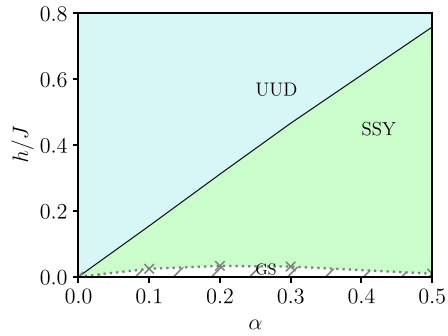


FIG. 8. The gs phase diagram h/J vs α obtained in this work, displaying three phases: the gapped spin solid (GS) phase for $h < h^*$, the supersolid Y (SSY) phase for $h_* < h < h_c$, and the polarized UUD phase on the magnetization plateau $h > h^*$.

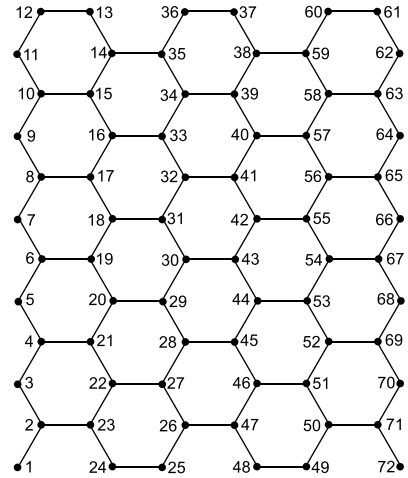


FIG. 9. HcL with $N = 72$ sites. A snakelike one-dimensional chain, constructed by following the numbering assigned to each site, is employed for the DMRG calculation.

leads to the effective AHM on a HcL but now (to keep the correspondence) at a finite external field h. Since the HcL is bipartite, its behavior is expected to be similar to the AHM on the SqL. Our numerical $T = 0$ results for $m(h)$ as well as for the transverse magnetization (corresponding to the supersolid parameter on the TL) $m_\perp(m)$ indeed reveal qualitative similarity to the full model on the TL, provided that we are restricted to the regime of correspondence, i.e., $1/2 \leqslant m \leqslant 1$, and to stronger anisotropy $\alpha \ll 1$. Nevertheless, in qualitative contrast with the AHM on the TL, both the HcL and SqL, even at the most interesting $m = 1/2$, indicate finite (although reduced) $m_\perp$, i.e., confirming gapless excitations in effective models.

This brings us back to the most challenging question of the vanishing $m_\perp$ and the related magnon gap $\Delta_1 > 0$ in the full TL model at $h = 0$. This also opens the possibility of a transition/crossover at $\alpha < 1$ since the isotropic case $\alpha = 1$ has quite well (even quantitatively) established $m_\perp > 0$. We present here additional results for magnon gaps $h^* = \Delta_1$, as they emerge at $T = 0$ from the analyses of $m(h)$ obtained from ED and DMRG results on systems up to $N = 72$ sites, covering the whole relevant range $\alpha < 1$ but as well some $\alpha < 0$ cases. Our analysis consistently reveals a decrease of the normalized gap Δ_1/α with increasing $\alpha < \alpha^* \sim 0.5$ as well as an asymmetry in $\alpha \to -\alpha$. Similar conclusions follow from the new calculation of the spin stiffness ρ_s, where extrapolated $N \to \infty$ results also indicate $\rho_s = 0$ (i.e., on a gapped solid) in the regime $\alpha < \alpha^* \sim 0.2$. The corresponding gs phase diagram, which emerges from our results (shown for $\alpha \leqslant 0.5$), is presented in Fig. 8, where in contrast with some previous studies (see, e.g., Ref. [14]), there is (quite a narrow regime of) a gapped spin-solid phase at $h < h^*(\alpha)$. Still, it seems to be beyond present numerical capabilities or analytical understading to clarify whether we are dealing with a transition or crossover at a particular α^*.

The absence of a supersolid in the TL model at small $\alpha \ll 1$ opens an evident question of the relation to previous results being in favor of the supersolid in the same regime. It should be recalled that one argument [12,13,30] emerges from the presumed symmetry of the model with respect to the sign of α in the Ising limit $|\alpha| \ll 1$. In fact, an ED calculation restricted to the degenerate Ising gs manifold (also referred to as the dimer model [12]) reveals, upon introduction of finite $|\alpha| \ll 1$, that excitations are symmetric upon $\alpha \to -\alpha$. Still, our results (for up to $N = 36$ sites) within this restricted problem are consistent with a finite magnon gap quite similar to the one obtained within the full model. This leads to a possible explanation that the asymmetry and the established supersolid at $\alpha < 0$ [9,11,30] emerge from higher orders/terms in α beyond the dimer model.

The emergence of the gap also indicates the qualitative failure of the LSWT in the $h \sim 0$ and $\alpha \ll 1$ regime. Although frequently used in the interpretation of experimental and numerical results, the LSWT has evident restrictions in $S = 1/2$ models. While starting at the finite magnetization plateau $m = 1/3$ for the TL, as well as with $m = 1$ for the HcL and SqL, the expansion in terms of magnons is well under control, the neglected terms (representing magnon repulsion) become the largest ones and apparently dominant at larger magnon densities, particularly at $m = 1/2$ for the HcL and SqL, and for $m = 0$ for the TL. The latter case corresponds to commensurate magnon filling, which together with strong magnon repulsion can lead to gap formation, in analogy with the Mott-insulator mechanism.

Finally, the main motivation for our study remains the recent fascinating experiments on the KCSO material [22–24]. While their overall interpretation in terms of the AHM of the TL with small $\alpha \sim 0.07$ is not in question, the possible indication of the gapped solid (at $h = 0$) instead of a supersolid requires further attention. Even in the available neutron-scattering results [23,24], the magnon spectra at the K point seem closer to the interpretation of a combination of quasielastic peak and gapped magnon excitation. Moreover, the measured (also calculated with QMC) magnetization curves $m(h)$ [24] show the tendency of flattening at $m \sim 0$ despite finite $T > 0$. Still, the main indication/confirmation would be an experimental measurement of $m_\perp(h)$, being a reachable challenge.

ACKNOWLEDGMENTS

We thank A. Zheludev for a stimulating discussion of recent experimental results. M.U. thanks J. Hofmann for

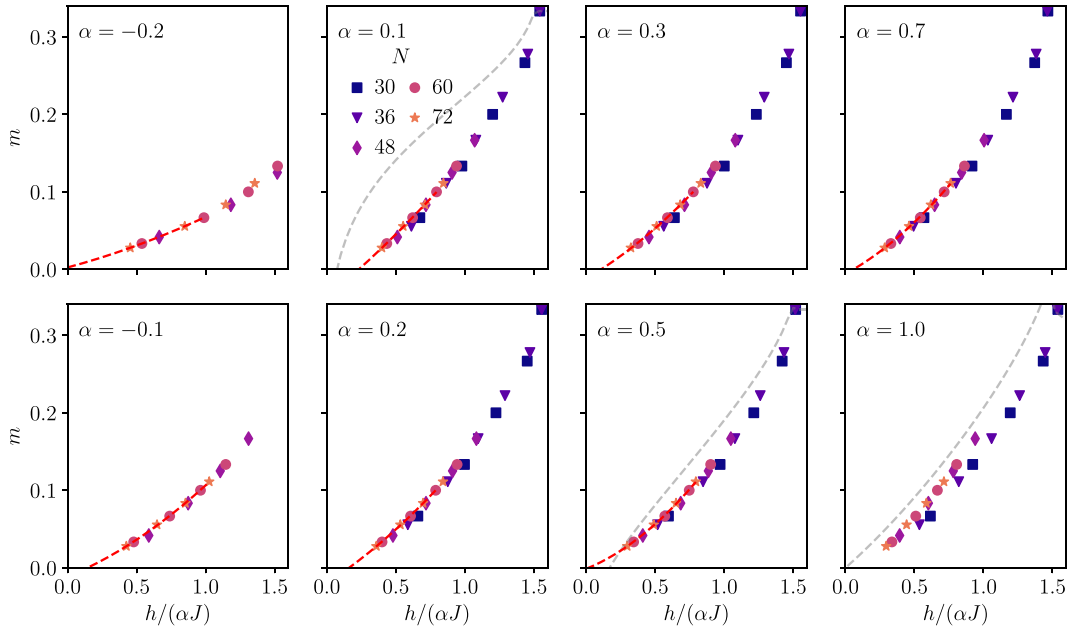


FIG. 10. Magnetization curves m vs normalized fields $h/(\alpha J)$ for various anisotropies $-0.2 \leqslant \alpha \leqslant 1$. The thin gray lines represent LSWT results, while the red lines are simple polynomial fits to the data for all cluster sizes N for small m. LSWT results for $\alpha = 1$ are obtained for coplanar classical spin orientations.

insightful discussions. This work is supported by the Slovenian Research and Innovation Agency (ARIS) under Program No. P1-0044 and Project No. J1-50008, and the JSPS KAKENHI (Grants No. 24K00560 and No. 25H01248) from the MEXT, Japan. A part of the computational work was performed using the computational resources of the supercomputer FUGAKU provided by the RIKEN Center for Computational Science through the HPCI System Research Project (Project ID No. hp250057). Parts of the ED calculation were performed by the XDiag library [45].

DATA AVAILABILITY

There are no publicly available research data or software supporting this manuscript. Requests for further information or data should be sent to the authors.

APPENDIX A: DMRG APPROACH

To perform DMRG on the HcL with $N = 72$, we construct a snakelike one-dimensional chain that runs from site 1 to site 72, as shown in Fig. 9. For a SqL with $N = 8 \times 8 = 64$, a similar one-dimensional mapping is employed (not shown). PBCs are imposed on both lattices. In the DMRG procedure, we set the maximum truncation number to $M = 8000$. After four sweeps, the resulting truncation error is less than 1×10^{-5}.

APPENDIX B: MAGNETIZATION CURVES

We present a larger set of results for the magnetization curves $m(h)$, covering the whole regime $-0.2 \leqslant \alpha \leqslant 1$, in Fig. 10, again obtained with ED for $N \leqslant 36$ and via DMRG and $N = 48, 60$, and 72 (restricted to $S^z_{\text{tot}} \leqslant 4$). We observe that, apart from the isotropic case $\alpha = 1$, the data from different N collapse quite well on a fitted curve. There is a notable difference between the data for positive and negative α, i.e., the magnetization curves for $\alpha < 0$ appear much shallower. For $\alpha = 1$, the data collapse is worse, signaling enhanced finite-size effects persisting up to $N = 72$, presumably requiring also different scaling with N for the isotropic case [46] and making an extrapolation $m \to 0$ less tractable.

[1] P. W. Anderson, Resonating valence bonds: A new kind of insulator? Mater. Res. Bull. **8**, 153 (1973).

[2] B. Bernu, P. Lecheminant, C. Lhuillier, and L. Pierre, Exact spectra, spin susceptibilities, and order parameter of the quantum Heisenberg antiferromagnet on the triangular lattice, Phys. Rev. B **50**, 10048 (1994).

[3] A. L. Chernyshev and M. E. Zhitomirsky, Spin waves in a triangular lattice antiferromagnet: Decays, spectrum renormalization, and singularities, Phys. Rev. B **79**, 144416 (2009).

[4] L. Capriotti, A. E. Trumper, and S. Sorella, Long-range Néel order in the triangular Heisenberg model, Phys. Rev. Lett. **82**, 3899 (1999).

[5] S. R. White and A. L. Chernyshev, Neel order in square and triangular lattice Heisenberg models, Phys. Rev. Lett. **99**, 127004 (2007).

[6] G. H. Wannier, Antiferromagnetism: The triangular Ising net, Phys. Rev. **79**, 357 (1950).

[7] S. Miyashita and H. Kawamura, Phase transitions of anisotropic Heisenberg antiferromagnets on the triangular lattice, J. Phys. Soc. Jpn. **54**, 3385 (1985).

[8] M. Boninsegni and N. V. Prokof'ev, Colloquium: Supersolids: What and where are they? Rev. Mod. Phys. **84**, 759 (2012).

[9] D. Heidarian and K. Damle, Persistent supersolid phase of hard-core bosons on the triangular lattice, Phys. Rev. Lett. **95**, 127206 (2005).

[10] M. Boninsegni and N. Prokof'ev, Supersolid phase of hard-core bosons on a triangular lattice, Phys. Rev. Lett. **95**, 237204 (2005).

[11] S. Wessel and M. Troyer, Supersolid hard-core bosons on the triangular lattice, Phys. Rev. Lett. **95**, 127205 (2005).

[12] F. Wang, F. Pollmann, and A. Vishwanath, Extended supersolid phase of frustrated hard-core bosons on a triangular lattice, Phys. Rev. Lett. **102**, 017203 (2009).

[13] H. C. Jiang, M. Q. Weng, Z. Y. Weng, D. N. Sheng, and L. Balents, Supersolid order of frustrated hard-core bosons in a triangular lattice system, Phys. Rev. B **79**, 020409(R) (2009).

[14] D. Yamamoto, G. Marmorini, and I. Danshita, Quantum phase diagram of the triangular-lattice XXZ model in a magnetic field, Phys. Rev. Lett. **112**, 127203 (2014).

[15] D. Sellmann, X.-F. Zhang, and S. Eggert, Phase diagram of the antiferromagnetic XXZ model on the triangular lattice, Phys. Rev. B **91**, 081104(R) (2015).

[16] N. Li, Q. Huang, X. Y. Yue, W. J. Chu, Q. Chen, E. S. Choi, X. Zhao, H. D. Zhou, and X. F. Sun, Possible itinerant excitations and quantum spin state transitions in the effective spin-1/2 triangular-lattice antiferromagnet $Na_2BaCo(PO_4)_2$, Nat. Commun. **11**, 4216 (2020).

[17] Y. Gao, Y. C. Fan, H. Li, F. Yang, X. T. Zeng, X. L. Sheng, R. Zhong, Y. Qi, Y. Wan, and W. Li, Spin supersolidity in nearly ideal easy-axis triangular quantum antiferromagnet $Na_2BaCo(PO_4)_2$, npj Quantum Mater. **7**, 89 (2022).

[18] J. Xiang, C. Zhang, Y. Gao, W. Schmidt, K. Schmalzl, C. W. Wang, B. Li, N. Xi, X. Y. Liu, H. Jin, *et al.*, Giant magnetocaloric effect in spin supersolid candidate $Na_2BaCo(PO_4)_2$, Nature (London) **625**, 270 (2024).

[19] Y. Gao, C. Zhang, J. Xiang, D. Yu, X. Lu, P. Sun, W. Jin, G. Su, and W. Li, Double magnon-roton excitations in the triangular-lattice spin supersolid, Phys. Rev. B **110**, 214408 (2024).

[20] T. Arh, B. Sana, M. Pregelj, P. Khuntia, Z. Jagličić, M. D. Le, P. K. Biswas, P. Manuel, L. Mangin-Thro, A. Ozarowski, *et al.*, The Ising triangular-lattice antiferromagnet neodymium heptatantalate as a quantum spin liquid candidate, Nat. Mater. **21**, 416 (2022).

[21] R. Zhong, S. Guo, and R. J. Cava, Frustrated magnetism in the layered triangular lattice materials $K_2Co(SeO_3)_2$ and $Rb_2Co(SeO_3)_2$, Phys. Rev. Mater. **4**, 084406 (2020).

[22] M. Zhu, V. Romerio, N. Steiger, S. D. Nabi, N. Murai, S. Ohira-Kawamura, K. Y. Povarov, Y. Skourski, R. Sibille, L. Keller, *et al.*, Continuum excitations in a spin-supersolid on a triangular lattice, Phys. Rev. Lett. **133**, 186704 (2024).

[23] T. Chen, A. Ghasemi, J. Zhang, L. Shi, Z. Tagay, Y. Chen, L. Chen, E. S. Choi, M. Jaime, M. Lee, *et al.*, Phase diagram and spectroscopic signatures of a supersolid in the quantum Ising magnet $K_2Co(SeO_3)_2$, Nat. Commun. **17**, 2914 (2026).

[24] M. Zhu, L. M. Chinellato, V. Romerio, N. Murai, Z. Yan, S. Gvasaliya, Y. Kato, C. D. Batista, and A. Zheludev, Wannier states and spin supersolid physics in the triangular antiferromagnet $K_2Co(SeO_3)_2$, npj Quantum Mater. **10**, 74 (2025).

[25] M. Ulaga, J. Kokalj, A. Wietek, A. Zorko, and P. Prelovšek, Finite-temperature properties of the easy-axis Heisenberg model on frustrated lattices, Phys. Rev. B **109**, 035110 (2024).

[26] M. Ulaga, J. Kokalj, T. Tohyama, and P. Prelovšek, Easy-axis Heisenberg model on the triangular lattice: From a supersolid to a gapped solid, Phys. Rev. B **111**, 174442 (2025).

[27] C. A. Gallegos, S. Jiang, S. R. White, and A. L. Chernyshev, Phase diagram of the easy-axis triangular-lattice J_1-J_2 model, Phys. Rev. Lett. **134**, 196702 (2025).

[28] Y. Xu, J. Hasik, B. Ponsioen, and A. H. Nevidomskyy, Simulating spin dynamics of supersolid states in a quantum Ising magnet, Phys. Rev. B **111**, L060402 (2025).

[29] R. Flores-Calderón, R. Moessner, and F. Pollmann, Unconventional spin dynamics and supersolid excitations in the triangular-lattice XXZ model, Phys. Rev. B **112**, 184423 (2025).

[30] R. G. Melko, A. Paramekanti, A. A. Burkov, A. Vishwanath, D. N. Sheng, and L. Balents, Supersolid order from disorder: Hard-core bosons on the triangular lattice, Phys. Rev. Lett. **95**, 127207 (2005).

[31] S. Toth and B. Lake, Linear spin wave theory for single-Q incommensurate magnetic structures, J. Phys.: Condens. Matter **27**, 166002 (2015).

[32] B. Kleine, P. Fazekas, and E. Müller-Hartmann, Perturbation theory for the triangular Heisenberg antiferromagnet with Ising-like anisotropy, Z. Phys. B **86**, 405 (1992).

[33] A. Mauri, S. Roose, and F. Mila, Non-linear spin wave theory in the strong easy-axis limit of the triangular XXZ model, Phys. Rev. B **113**, 174433 (2026).

[34] M. Holtschneider, S. Wessel, and W. Selke, Classical and quantum two-dimensional anisotropic Heisenberg antiferromagnets, Phys. Rev. B **75**, 224417 (2007).

[35] A. Honecker, A comparative study of the magnetization process of two-dimensional antiferromagnets, J. Phys.: Condens. Matter **11**, 4697 (1999).

[36] A. Honecker, J. Schulenburg, and J. Richter, Magnetization plateaus in frustrated antiferromagnetic quantum spin models, J. Phys.: Condens. Matter **16**, S749 (2004).

[37] P. Prelovšek and J. Bonča, Ground state and finite temperature Lanczos methods, in *Strongly Correlated Systems—Numerical Methods*, edited by A. Avella and F. Mancini (Springer, Berlin, 2013).

[38] E. Manousakis, The spin-½ Heisenberg antiferromagnet on a square lattice and its application to the cuprous oxides, Rev. Mod. Phys. **63**, 1 (1991).

[39] J. Bonča, J. P. Rodriguez, J. Ferrer, and K. S. Bedell, Direct calculation of spin stiffness for spin-1/2 Heisenberg models, Phys. Rev. B **50**, 3415 (1994).

[40] P. Lecheminant, B. Bernu, C. Lhuillier, and L. Pierre, Spin stiffnesses of the quantum Heisenberg antiferromagnet on a triangular lattice, Phys. Rev. B **52**, 9162 (1995).

[41] S. E. Krüger, R. Darradi, J. Richter, and D. J. J. Farnell, Direct calculation of the spin stiffness of the spin-$\frac{1}{2}$ Heisenberg antiferromagnet on square, triangular, and cubic lattices using the coupled-cluster method, Phys. Rev. B **73**, 094404 (2006).

[42] W. Kohn, Theory of the insulating state, Phys. Rev. **133**, A171 (1964).

[43] D. J. Scalapino, S. R. White, and S. Zhang, Insulator, metal, or superconductor: The criteria, Phys. Rev. B **47**, 7995 (1993).

[44] M. E. Zhitomirsky and T. Nikuni, Magnetization curve of a square-lattice Heisenberg antiferromagnet, Phys. Rev. B **57**, 5013 (1998).

[45] A. Wietek, L. Staszewski, M. Ulaga, P. L. Ebert, H. Karlsson, S. Sarkar, H. Shackleton, A. Sinha, and R. D. Soares, Xdiag: Exact diagonalization for quantum many-body systems, SciPost Phys. Codebases 70 (2026).

[46] D. A. Huse, Ground-state staggered magnetization of two-dimensional quantum Heisenberg antiferromagnets, Phys. Rev. B **37**, 2380 (1988).